

Microscopic Viscoelasticity of Polymer Solutions and Gels Observed from Translation and Rotation of Anisotropic Colloid Probes

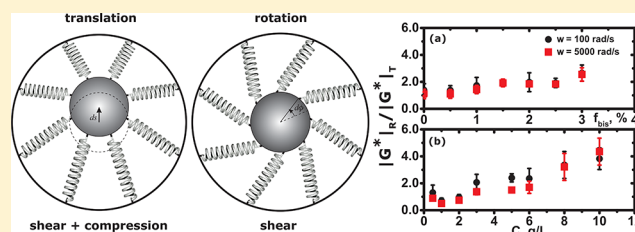
Carlos Gutiérrez-Sosa,[†] Arturo Merino-González,[‡] Rodrigo Sánchez,[†] Anna Kozina,^{*,‡,§} and Pedro Díaz-Leyva[†]

[†]Departamento de Física, Universidad Autónoma Metropolitana Iztapalapa, San Rafael Atlixco 186, 09340 Mexico City, Mexico

[‡]Instituto de Química, Universidad Nacional Autónoma de México, P.O. Box 70-213, 04510 Mexico City, Mexico

Supporting Information

ABSTRACT: We probe the mechanics of two different viscoelastic complex systems at a microscopic length scale. The first is made of cross-linked polymer gel, and the second consists of a polysaccharide solution, in which spherical birefringent colloidal tracers have been embedded. This method is widely known as optical microrheology. In the present work we focus on both the translational and the rotational motions of the tracers. The significant discrepancies observed between the results obtained by translational and rotational microrheology imply that the two types of motion probe the mechanical response of the matrix in different ways. We also suggest a simplified theoretical model to explain the experimentally observed discrepancies in terms of the relationship between the viscoelastic moduli obtained from rotational and translational tracer dynamics. Our results have implications for the insights obtainable by rotational and translational microrheology and for the role of compressibility.



I. INTRODUCTION

Microrheology is a technique that has been used for over two decades to characterize micromechanical properties of soft materials, which are of interest in science, industry, and medicine. It is based on tracking of diffusion of a probe particle in a viscoelastic medium. In the early reported works, the translational dynamics of colloidal tracers using diffusive wave spectroscopy (DWS) and dynamic light scattering (DLS) were measured.^{1–3} This technique became popular and is widely used to characterize colloidal suspensions, emulsions, polymer solutions, surfactant micellar fluids, biological tissues, and more complex soft matter systems.^{4–7,12} Later, works with a focus on rotational dynamics of colloidal tracers were reported.^{8–11} The dynamics of optically anisotropic spherical tracers can be studied by depolarized dynamic light scattering (DDLS), and the viscoelastic properties may be extracted as well from the particle time-dependent angular displacement. The latter technique is known as rotational microrheology.

Traditionally, the results of translational microrheology were compared with those obtained by mechanical bulk rheology to validate them. Indeed, for some viscoelastic systems bulk and microrheology results matched quite well.^{12–16} However, in the case of more complex systems such as colloidal glasses and gels, cross-linked polymer gels, and biological tissues, a disagreement between the two techniques was observed.^{6,17–21} This is due to the fact that the local viscoelastic response does not always reflect the macroscopic properties. Moreover, the system characteristics such as structural and dynamic heterogeneities, the tracer size as compared to the characteristic length of the medium, and tracer–medium interactions

also influence the observed tracer dynamics and, as a result, microscopic viscoelastic properties.^{17,19,22–26}

In a homogeneous viscous medium the translation and rotation of a spherical particle are coupled, so that the ratio of the corresponding mean-square displacements (MSD) $\langle \delta r^2(t) \rangle / \langle \delta \theta^2(t) \rangle$ is a constant. As the particle diffusion slows down, for example due to particle trapping in a matrix, the rotation may decouple from translation; namely, the ratio of the two MSDs ceases to be a constant. Therefore, the microrheological response obtained by the two types of motion might not coincide, assuming that under equilibrium conditions they should provide the same response. The decoupling of translation from rotation was previously observed for simple liquids and colloidal suspensions approaching the glass transition,^{27–32} for gels made of alumina crystals in fatty acids,³³ and for semidilute xanthan solutions.³⁴ On comparison of the viscoelastic moduli observed by translational and rotational dynamics of tracers, both agreement and disagreement are reported for a few tracer–matrix systems.^{8–11} Apart from a few reports on comparison of the two types of responses, no systematic study has been done on the influence of “sticky” tracer–polymer interactions on the viscoelastic properties observed by translational and rotational microrheology.

In the present work we show that under conditions of dynamical arrest the compressibility of the polymer matrix

Received: May 14, 2018

Revised: October 27, 2018

Published: November 8, 2018

causes a gradual decoupling of rotational and translational tracer diffusion. Such a decoupling is expressed as a difference in the viscoelastic moduli obtained by rotational and translational microrheology. As a model to test such a decoupling, we use two different polymeric matrices. The first system is polyacrylamide (PAA) aqueous sols and gels with a tendency to adsorb on the cross-linked liquid crystal spherical, optically anisotropic probe particles. The mesh size of such a polymer matrix is much smaller than the probe size, and the matrix can therefore be treated as a continuum. We vary the degree of cross-linking arresting the tracer motion. The second system is semidilute and concentrated aqueous solutions of semirigid xanthan polysaccharide at high ionic strength. This polysaccharide has an ordered double-helical conformation at room temperature and high ionic strength.³⁵ Xanthan has a strong tendency to aggregate due to hydrogen bonding,³⁶ and it readily adsorbs on our probe particles, although to lesser extent than PAA. In both cases, entropy may favor adsorption.^{37,38} Therefore, this system also fulfills the no-slip probe–matrix condition. The characteristic correlation length of xanthan solutions is higher than that of PAA sols and gels, and at lower xanthan concentration it is about 30% less than the tracer size. Nevertheless, despite the medium difference, in both cases the decoupling of the two tracer dynamics occurs on slowing down of the probe diffusion motion. We suggest a simple-model theory that relies on the no-slip condition between the tracer and the matrix and takes into account polymer compressibility to explain discrepancies in viscoelastic moduli observed by different tracer motions.

II. EXPERIMENTAL SECTION

II.A. Materials. Absolute ethanol was purchased from J.T. Baker. Sodium dodecyl sulfate (SDS), xanthan polysaccharide (G1253), 2-hydroxy-2-methylpropiophenone (Darocur 1173), sodium chloride, acrylamide (AA), *N,N'*-methylenebis(acrylamide) (BA), ammonium persulfate, and *N,N,N',N'*-tetramethylethylenediamine (TEMED) were purchased from Sigma-Aldrich. Reactive Mesogen 257 (RM 257) was supplied by Xi'an Caijing Opto-Electrical Science & Technology Co., Ltd., China. All the compounds except for xanthan were used without further purification. Deionized water (Milli-Q, resistivity $\rho = 18.1 \text{ M}\Omega\cdot\text{cm}$) was used.

II.B. Synthesis of Optically Anisotropic Colloidal Tracers. Liquid crystal particles (LCP) were synthesized by a previously reported procedure.³⁹ A solution of 40 mg of RM 257 and 20 mg of Darocur 1173 in 5 g of ethanol was prepared and quickly added to a hot solution (70 °C) of 0.46 g of SDS in 200 mL of water under constant ultrasonication. An emulsion was formed within a few minutes and was left in ultrasonication for 1 h at 70 °C. The emulsion droplets were then solidified by UV-light illumination on gentle stirring at 70 °C. The solid particles were washed with water to remove excess SDS. Particle geometrical R_{dry} and hydrodynamic R_{h} radii as well as the polydispersity index PDI were characterized by scanning electron microscopy (SEM) and depolarized dynamic light scattering (DDLS). The hydrodynamic radius was characterized both in water and in an aqueous 0.1 M NaCl solution. The following LCP tracer characteristics were obtained: $R_{\text{dry}} = 159.7 \text{ nm}$, polydispersity PDI = 3.3%, $R_{\text{h}} = 175.3 \text{ nm}$ in water, and $R_{\text{h}} = 169.4 \text{ nm}$ in 0.1 M NaCl aqueous solution.

II.C. Sample Preparation. Cross-linked networks consisted of PAA chains cross-linked with *N,N'*-methylenebis(acrylamide) (BA). Ammonium persulfate and TEMED were used as reaction initiator and catalyst, respectively. A standard procedure was used to prepare polyacrylamide gels as in molecular biology for protein electrophoresis.⁴⁰ The extent of cross-linking depends on the fraction $f_{\text{bis}} = [\text{BA}]/([\text{AA}] + [\text{BA}])$. In the present work f_{bis} was varied in the range of 0–3% w/w, keeping the total amount of monomers $[\text{AA}] + [\text{BA}] =$

2.5% w/w for all samples. LCP tracers were dispersed in the monomer solution before polymerization, which was performed at room temperature directly in light scattering cells. The measurements were made 48 h after sample preparation. The range of values of f_{bis} was chosen to cover the sol–gel transition.⁴¹ The LCP tracers volume fraction was fixed at about 10^{-5} to avoid interparticle interactions and multiple scattering.

Xanthan was purified from large aggregates as previously reported.³⁶ Xanthan samples were prepared by dissolution of the desired amount of the purified polymer in 0.1 M solution of NaCl containing 0.02% w/w NaN_3 (antimicrobial agent) and followed by its renaturalization. The amount of tracer particles was adjusted for each polymer concentration to obtain sufficient signal-to-noise ratio with the maximum volume fraction of 2×10^{-4} . The samples without tracers did not present light scattering in the cross-polarized mode, indicating the absence of optically anisotropic objects.

II.D. Characterization by Depolarized Dynamic Light Scattering. DDLS experiments were performed with a 3D light scattering spectrometer (LS Instruments, Switzerland) in a pseudo-cross-correlation mode using a HeNe laser with the wavelength $\lambda = 632.8 \text{ nm}$ equipped with two Glan-Thompson linear polarizers. A vertically polarized laser beam is focused on the sample cell. The second polarizer is located in front of the optical fiber and is perpendicular (horizontal) relative to the first one to ensure that only the signal from the depolarized scattering (VH) reaches the APD detectors (Excelitas, Canada). The depolarized time-averaged autocorrelation function of the scattered intensity $g_2^{\text{VH}}(q, \tau)$ is measured at a certain scattering angle θ . Here q is the wave vector given by $q = (4\pi n/\lambda) \sin(\theta/2)$ with n denoting the refractive index of the medium. Applying Siegert's relation⁴² for ergodic samples or the Pusey–van Meegen procedure of correction for the nonergodicity,⁴³ one obtains the depolarized intermediate scattering function $f_{\text{VH}}(q, \tau)$ (DISF) from $g_2^{\text{VH}}(q, \tau)$. In the measured DISF the translational and rotational contributions to the particle dynamics are mixed according to⁴⁴

$$f_{\text{VH}}(q, \tau) = e^{-q^2 W(\tau)} e^{-6\Omega(\tau)} \quad (1)$$

where the subindex VH denotes crossed polarizers and $W(t)$ and $\Omega(t)$ are the translational and rotational self-diffusion coefficients, respectively. These are related to the corresponding translational (TMSD) and rotational (RMSD) mean-square displacements as $W(t) = \langle \delta r^2(t) \rangle / 6$ and $\Omega(t) = \langle \delta \theta^2(t) \rangle / 4$. To separate the two contributions, the measurements at the two different angles θ_1 and θ_2 can be done with the corresponding scattering vectors q_1 and q_2 . Then, one can obtain the MSDs as follows:

$$\langle \delta r^2(t) \rangle = \frac{6}{q_2^2 - q_1^2} \ln \left| \frac{f_{\text{VH}}(q_1, \tau)}{f_{\text{VH}}(q_2, \tau)} \right| \quad (2)$$

$$\langle \delta \theta^2(t) \rangle = \frac{2}{3(q_2^2 - q_1^2)} \ln \left| \frac{[f_{\text{VH}}(q_2, \tau)]^{q_1^2}}{[f_{\text{VH}}(q_1, \tau)]^{q_2^2}} \right| \quad (3)$$

II.E. Microrheological Concepts for Translational and Rotational Dynamics of Tracers. For colloidal particles of radius a immersed in a viscoelastic medium described by a complex modulus $G^*(\omega)$, the translational generalized Stokes–Einstein relation is given by²

$$G_T^*(\omega) = \frac{k_B T e^{[i\pi\alpha_T(\omega)]/2}}{\pi a \langle \delta r^2(1/\omega) \rangle \Gamma[1 + \alpha_T(\omega)]} \quad (4)$$

where $k_B T$ is the thermal energy. The rotational counterpart of eq 4 is given by¹⁰

$$G_R^*(\omega) = \frac{k_B T e^{[i\pi\alpha_R(\omega)]/2}}{4\pi a^3 \langle \delta \theta^2(1/\omega) \rangle \Gamma[1 + \alpha_R(\omega)]} \quad (5)$$

where $\alpha_T(\omega)$ and $\alpha_R(\omega)$ are logarithmic derivatives of TMSD and RMSD, respectively, evaluated at $t = 1/\omega$, given as

$$\alpha_T(\omega) = \left. \frac{d \log \langle \delta r^2(t) \rangle}{d \log t} \right|_{t=1/\omega} \quad (6)$$

$$\alpha_R(\omega) = \left. \frac{d \log \langle \delta \theta^2(t) \rangle}{d \log t} \right|_{t=1/\omega} \quad (7)$$

Using Euler's equation for eqs 4 and 5, one obtains

$$G'_{T/R}(\omega) = |G_{T/R}^*(\omega)| \cos\left(\frac{\pi\alpha_{T/R}(\omega)}{2}\right) \quad (8)$$

$$G''_{T/R}(\omega) = |G_{T/R}^*(\omega)| \sin\left(\frac{\pi\alpha_{T/R}(\omega)}{2}\right) \quad (9)$$

with the subscript T/R meaning either translational or rotational quantity. Here

$$|G_T^*(\omega)| \approx \frac{k_B T}{\pi a \langle \delta r^2(1/\omega) \rangle \Gamma[1 + \alpha_T(\omega)]} \quad (10)$$

and

$$|G_R^*(\omega)| \approx \frac{k_B T}{4\pi a^3 \langle \delta \theta^2(1/\omega) \rangle \Gamma[1 + \alpha_R(\omega)]} \quad (11)$$

The comparison of the moduli obtained by translational and rotational tracer motion can be done in terms of the ratio $G_T^*(\omega)/G_R^*(\omega)$. Consider two time regimes for an arrested viscoelastic medium: (a) very short times, when a tracer moves almost freely, and (b) very long times, when a tracer motion is dynamically arrested. For the first case, the parameter $\alpha(\omega)$ tends to be 1 at the time regime $t \rightarrow 0$ (or similarly when $\omega \rightarrow \infty$); as a consequence $G_T'(\omega \rightarrow \infty) = G_R'(\omega \rightarrow \infty) = 0$, and it yields

$$\frac{G_T^*(\omega \rightarrow \infty)}{G_R^*(\omega \rightarrow \infty)} = \frac{G_T''(\omega \rightarrow \infty)}{G_R''(\omega \rightarrow \infty)} \quad (12)$$

When $\alpha_T(\omega) = \alpha_R(\omega) = 1$, $\Gamma[1 + \alpha_T(\omega)] = \Gamma[1 + \alpha_R(\omega)] = \Gamma[2] = 1$, and as a consequence

$$\frac{G_T''(\omega \rightarrow \infty)}{G_R''(\omega \rightarrow \infty)} = 4a^2 \frac{\langle \delta \theta^2(t \rightarrow 0) \rangle}{\langle \delta r^2(t \rightarrow 0) \rangle} \quad (13)$$

In the second case, $\alpha(\omega)$ tends to be 0 at the time regime $t \rightarrow \infty$ (or similarly when $\omega \rightarrow 0$); as a consequence $G_T''(\omega \rightarrow 0) = G_R''(\omega \rightarrow 0) = 0$, and it yields

$$\frac{G_T^*(\omega \rightarrow 0)}{G_R^*(\omega \rightarrow 0)} = \frac{G_T'(\omega \rightarrow 0)}{G_R'(\omega \rightarrow 0)} \quad (14)$$

When $\alpha_T(\omega) = \alpha_R(\omega) = 0$, $\Gamma[1 + \alpha_T(\omega)] = \Gamma[1 + \alpha_R(\omega)] = \Gamma[1] = 1$, and as a consequence

$$\frac{G_T'(\omega \rightarrow 0)}{G_R'(\omega \rightarrow 0)} = 4a^2 \frac{\langle \delta \theta^2(t \rightarrow \infty) \rangle}{\langle \delta r^2(t \rightarrow \infty) \rangle} \quad (15)$$

Equations 13 and 15 imply that when the mean-square displacements are coupled (their ratio is a constant), the ratio of the moduli obtained by translational and rotational tracer motion is unity, and therefore translational and rotational microrheologies provide the same results. However, the latter consideration does not take into account possible decoupling of the translation from rotation, which we will discuss further.

III. RESULTS AND DISCUSSION

III.A. Cross-Linked Polyacrylamide Networks and Xanthan Solutions. Figures 1 and 2 show translational and rotational mean-square displacements of tracer particles in pure water, 0.1 M NaCl, PAA sols and gels, and xanthan solutions on increase of the cross-linker fraction f_{bis} or xanthan

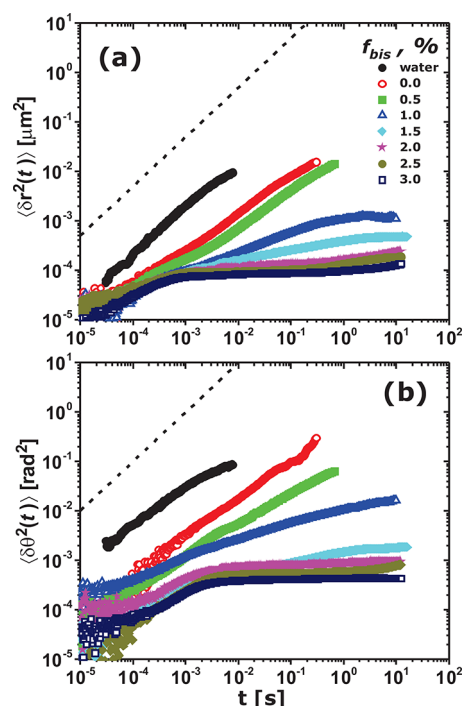


Figure 1. Translational (a) and rotational (b) MSD of the tracers in PAA networks on variation of cross-linker mass fraction f_{bis} as given in the legend. The black dashed line indicates a slope of unity.

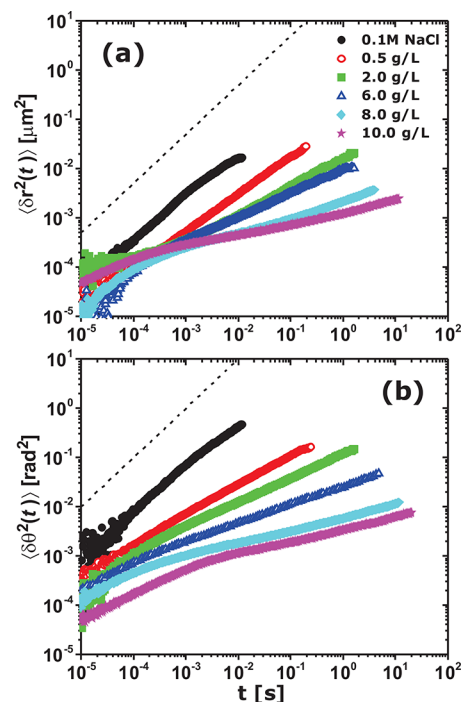


Figure 2. Translational (a) and rotational (b) MSD of the tracers in xanthan 0.1 M NaCl solutions on variation of polymer concentration as given in the legend. The black dashed line indicates a slope of unity.

concentration. The corresponding time correlation functions of depolarized scattered electric field are shown in the Supporting Information (Figure S1).

As can be seen in Figure 1, particle diffusion is free in water, and it slows down in the polymer sol up to $f_{\text{bis}} = 1.0$. When the

polymer gel is formed, $f_{\text{bis}} > 1.5$, the tracer dynamics are arrested, which is consistent with gel formation. At $f_{\text{bis}} \approx 1.0$ – 1.5 intermediate dynamics are observed, reflecting the vicinity of the sol–gel transition. The particle dynamics in xanthan solutions (Figure 2) is free up to 2.0 g/L, and then it gradually slows down, showing two distinct dynamic time scales with different slopes at short and long times. Even for the largest xanthan concentration the plateau at long times is still absent indicating faster tracer dynamics than in PAA gels.

The absolute value of the complex moduli $|G_T^*|$ and $|G_R^*|$ obtained from these MSDs are shown in Figures 3 and 4 for selected f_{bis} and xanthan concentrations. The corresponding viscoelastic moduli G' and G'' are shown in the Supporting Information (Figure S2).

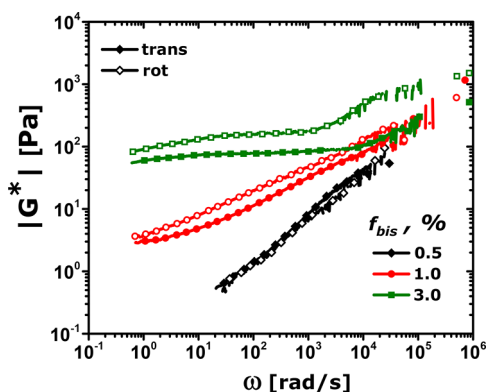


Figure 3. Absolute values of the complex moduli $|G_T^*|$ (filled symbols) and $|G_R^*|$ (open symbols) obtained from translational and rotational MSDs of the tracers in PAA networks on variation of the cross-linker mass fraction f_{bis} as given in the legend.

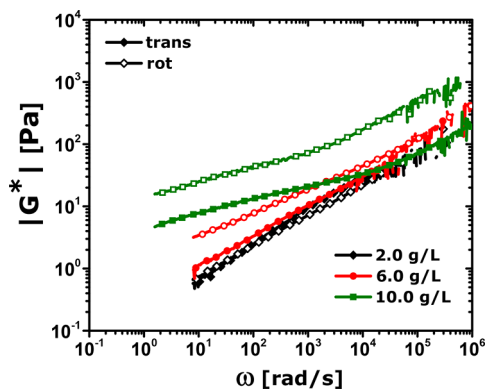


Figure 4. Absolute values of the complex moduli $|G_T^*|$ (filled symbols) and $|G_R^*|$ (open symbols) obtained from translational and rotational MSDs of the tracers in xanthan solutions at three concentrations given in the legend.

As the cross-link density increases, the system behaves first as a viscous liquid and, after the sol–gel transition, it turns into an elastic solid. Such a behavior is typical for sols turning into chemically cross-linked strong gels. In all the cases the moduli obtained from the rotational motion are larger than those from the translational one. The difference between the moduli is the smallest at the lowest cross-link density, and it increases with increasing polymer cross-linking. As can be seen in Figure 4, for xanthan saline solutions both moduli increase monotonically as frequency increases. Such a behavior is typical for semidilute and concentrated xanthan solutions at room

temperature. For high concentrations G' is larger than G'' in the whole frequency range (see the Supporting Information), and both moduli depend only slightly on the oscillation frequency. This behavior is attributed to a weak gel and is similar to previously observed behavior in bulk rheology.^{45–48} At lower concentration, the storage and the loss moduli are practically equal, which characterizes the transition from the fluidlike to the solidlike behavior or the concentration regime at the onset of structure formation. In this regime the moduli obtained from rotational tracer motion reproduce the translational moduli. With an increase of xanthan concentration, $|G_R^*|$ increases as compared to $|G_T^*|$, similar to the case of PAA gels in Figure 3.

In a homogeneous viscous medium translational and rotational motions of tracers are coupled, and the ratio $\langle \delta r^2(t) \rangle / \langle \delta \theta^2(t) \rangle$ is expected to be a constant. The ratio $|G_R^*| / |G_T^*|$ tends to unity, and therefore one expects a good agreement between the observed moduli.^{8,10} On increase of the medium's rigidity, the tracer dynamics slow down so that the rotation may decouple from translation. We observe such a decoupling in our experiments at large cross-linked density of PAA gels or xanthan concentrations (see Figure S5). Because the ratio of the mean-square displacements is not a constant, the ratios of the complex moduli are not expected to tend to unity; namely, there should be a disagreement between the viscoelastic response to each type of tracer motion. The larger moduli observed by the rotational motion in Figures 3 and 4 imply that the tracer rotation is more restrained than its translation. We attribute this fact to the difference in the matrix response to the two types of motion, in which tracer–matrix interactions and polymer compressibility could play an important role.

Liquid crystal tracer particles consist of chemically linked monomers of RM 257 aligned in parallel to the nematic director, as shown in Figure S6. The measurement of ζ -potential of these particles in water yields -13.8 ± 1.8 mV. The small negative charge in water is probably due to the presence of carboxylated ester groups or reduced carbonyl groups as a result of radical transfer in water during the polymerization process, although the exact surface chemistry of these particles has not been reported. To confirm the presence of interactions between LCP tracers and the studied polymers we performed adsorption experiments. The LCP tracers were dispersed in an aqueous solution of linear PAA (sample with $f_{\text{bis}} = 0$) and saline xanthan solution with $C = 0.2$ g/L. After 24 h of stirring at room temperature the particles were cleaned by 15 cycles of sedimentation–redispersion procedure to remove excess nonadsorbed polymer. Afterward, the hydrodynamic radius and the ζ -potential of the particles in water were measured. The corresponding DISFs for the particles in water before and after polymer adsorption are given in Figure S6. The hydrodynamic radius obtained from the corresponding DISFs after PAA adsorption is 395.3 nm and after xanthan adsorption is 219.4 nm. The corresponding ζ -potentials are -16.1 ± 2.1 and -29.7 ± 2.2 mV. These results suggest that both PAA and xanthan adsorb onto the tracer surface, which increases the particle radius and the ζ -potential. A change in ζ -potential is more pronounced for xanthan because of its polyanionic nature. For the same reason it adsorbs less than PAA does on slightly negatively charged particles. Polymer adsorption indicates that the tracer particles do interact with both polymers and such interactions cannot be neglected when probing microrheological response. Although the precise

mechanism and nature of these interactions is beyond the scope of the present work, the following may contribute to the polymer adsorption on our tracer particles: hydrogen bonding, hydrophobic interactions, and van der Waals attraction.^{49–52} In addition, the fact that adsorption is entropically favorable^{37,38} and that it decreases solid–liquid interfacial tension likely contribute to polymer adsorption. As a result, a certain number of particle–matrix contacts are formed, the situation akin to a sphere trapped in a 3D spider web. The number of such polymer-on-particle adsorption sites depends on the polymer concentration and is related to the matrix mesh size. The mesh size ξ of the polymer network may be estimated as $\xi = R_G(C^*/C)^{3/4}$,⁵³ where R_G is the radius of gyration and C and C^* are the polymer concentration and its critical value, respectively. For PAA solutions with 2.5% w/w polymer concentration it is estimated to be less than 10 nm.⁹ For our xanthan solutions in the range 2–10 g/L it varies from 116 to 35 nm. Therefore, in the both cases, the tracer size is well above the mesh size of the polymer matrix except for the most dilute xanthan solutions, in which we observe an agreement between the two types of moduli. On increase of the polymer or cross-linker concentration, the LCP tracer motion becomes more restrained. Because of the tracer–matrix interactions, our system is different from the others where the particles rotate in a “cavity” made by their nearest neighbors or due to depletion of the polymer matrix from the volume close to the tracer surface.^{24,26,31,34} Therefore, in our case the tracer–matrix interactions introduce a difference in the tracer motion decoupling as compared to some of the previously studied systems; namely, rotation slows down faster than translation.

The rotation–translation decoupling can be well represented by the ratios in the complex moduli $|G_R^*|/|G_T^*|$ at a given radial frequency. Figure 5 shows these ratios for PAA and

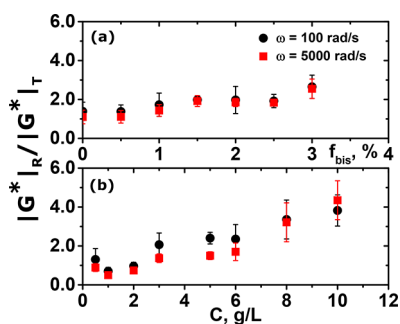


Figure 5. Ratios of viscoelastic complex moduli obtained by rotational and translational motion of the tracers $|G_R^*|/|G_T^*|$: (a) PAA sols and gels on variation of f_{bis} and (b) xanthan solutions on variation of its concentration. The values correspond to frequencies of 100 (circles) and 5000 rad/s (squares).

xanthan solutions and gels as a function of the cross-linker mass fraction (PAA) and concentration (xanthan). For the studied range of frequencies rotational moduli are almost always larger than translational ones, except for non-cross-linked PAA sols and low concentration xanthan solutions. An increase of the cross-linking in PAA networks results in an increase of this difference, especially for $f_{bis} > 1.5\%$. This implies that the tracer motion decoupling is more pronounced at larger cross-linking and elasticity of the gels, probably because of the stronger tracer confinement in the gel network. A similar trend is observed on increase of xanthan concentration. Both elastic and viscous moduli from rotational

motion are greater than those from translational one. Their difference grows with an increase of structure formation as one moves to more concentrated polysaccharide solutions, once more confirming the role of the tracer confinement in its motion decoupling. At the lowest xanthan concentrations (up to 2.0 g/L) the ratios smaller than one are observed most probably due to low sample elasticities and large mesh size, which may lead to a partial tracer slippage on rotation. To tackle the problem of tracer motion decoupling as well as to find a possible reason for more restrained rotation as compared to translation, we suggest the following theoretical model.

III.B. Viscoelastic Continuous No-Slip Model. Let us consider a model as depicted in Figure 6. A rigid tracer sphere

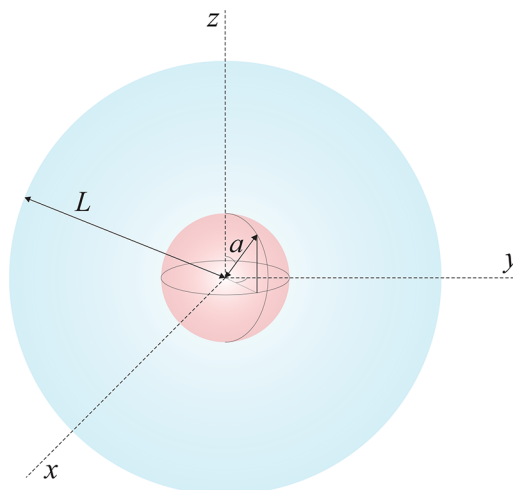


Figure 6. Schematic representation of the proposed model. A tracer sphere of radius a trapped inside a sphere of radius L made of a viscoelastic material with shear modulus G and shear viscosity η .

of radius a is trapped inside a larger sphere of radius L ($L \gg a$). The large sphere is made of an isotropic and homogeneous material (medium) with the shear modulus G and shear viscosity η . We can reasonably assume that the medium is nearly incompressible (the solvent can be assumed to be incompressible, while the gel network may be compressible^{25,54}) and that it responds to the tracer motion according to the no-slip boundary condition. The tracer sphere undergoes translational and rotational displacements by a distance s and by an angle σ , respectively.

B.1. Translational Displacement by a Distance s . Figure 7 shows a schematic representation of the translational displacement. The tracer sphere is displaced along the z -axis by a distance s without rotation. The displacement of an arbitrary infinitesimal element of surface area $dA = a^2 \sin \theta d\theta d\phi$ by s results in both shear and normal stresses. Because both shear and normal stresses counteract the displacement, the work done on any element of the surface area is the modulus of the force opposing the motion multiplied by ds . Thus, the total work can be obtained by considering the total force over the entire surface and integrating over the displacement. The total force exerted on a surface infinitesimal element dA during a displacement by a distance s is given by

$$dF_s = \sqrt{\tau_{\parallel}^2 + \tau_{\perp}^2} dA \quad (16)$$

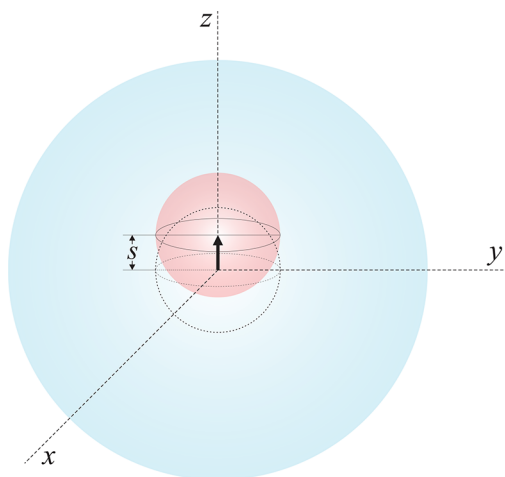


Figure 7. Probe has executed a linear displacement by a distance s along the z -axis inside a medium with shear modulus G and shear viscosity η .

where τ_{\parallel} and τ_{\perp} are the shear and the normal stress, respectively. For a Hookean solid (elastic contribution) the stresses can be expressed as

$$\tau_{\parallel}^{(E)} = \gamma_{\parallel} G = G \frac{s \sin \theta}{L} \quad (17)$$

$$\tau_{\perp}^{(E)} = \gamma_{\perp} Y = Y \frac{s \cos \theta}{L} \quad (18)$$

where G is the shear modulus, Y is the Young's modulus, and γ_{\parallel} and γ_{\perp} are shear and normal strains, respectively. For a Newtonian fluid (viscous contribution) the stresses are

$$\tau_{\parallel}^{(V)} = \eta \dot{\gamma}_{\parallel} = \eta \frac{v \sin \theta}{L} \quad (19)$$

$$\tau_{\perp}^{(V)} = \eta_{\text{ext}} \dot{\gamma}_{\perp} = \eta_{\text{ext}} \frac{v \cos \theta}{L} \quad (20)$$

where v is the speed of tracer displacement, η is the shear viscosity, η_{ext} is the extensional viscosity, and $\dot{\gamma}_{\parallel}$ and $\dot{\gamma}_{\perp}$ are the shear and normal rates, respectively. Combining eqs 16, 17, and 18, the force for the elastic contribution $dF_s^{(E)}$ can be rewritten as

$$dF_s^{(E)} = \frac{s}{L} \sqrt{G^2 \sin^2 \theta + Y^2 \cos^2 \theta} a^2 \sin \theta \, d\theta \, d\phi \quad (21)$$

In a similar way combining eqs 16, 19, and 20, the force for the viscous contribution $dF_s^{(V)}$ is

$$dF_s^{(V)} = \frac{v}{L} \sqrt{\eta^2 \sin^2 \theta + \eta_{\text{ext}}^2 \cos^2 \theta} a^2 \sin \theta \, d\theta \, d\phi \quad (22)$$

For a nearly Hookean isotropic weakly compressible solid, the relationship between Young's modulus Y and shear modulus G is $Y \approx 3G$.⁵⁵ In a similar way, for a purely Newtonian isotropic incompressible liquid, the relationship between extensional viscosity η_{ext} and shear viscosity η is $\eta_{\text{ext}} = 3\eta$. Equations 21 and 22 thus become

$$dF_s^{(E)} = \frac{Gsa^2}{L} \sqrt{1 + 8 \cos^2 \theta} \sin \theta \, d\theta \, d\phi \quad (23)$$

$$dF_s^{(V)} = \frac{\eta va^2}{L} \sqrt{1 + 8 \cos^2 \theta} \sin \theta \, d\theta \, d\phi \quad (24)$$

Integration of eqs 23 and 24 yields

$$F_s^{(E)} = G \frac{2\pi a^2 s}{L} \left[3 + \frac{\tanh^{-1}\left(\frac{2\sqrt{2}}{3}\right)}{2\sqrt{2}} \right] \quad (25)$$

$$F_s^{(V)} = \eta \frac{2\pi a^2 v}{L} \left[3 + \frac{\tanh^{-1}\left(\frac{2\sqrt{2}}{3}\right)}{2\sqrt{2}} \right] \quad (26)$$

The work is obtained by integration of eqs 25 and 26. The work for the elastic contribution is then

$$W_s^{(E)} = G \frac{\pi a^2 s^2}{L} \left[3 + \frac{\tanh^{-1}\left(\frac{2\sqrt{2}}{3}\right)}{2\sqrt{2}} \right] \quad (27)$$

and for the viscous contribution is

$$W_s^{(V)} = \eta \frac{2\pi a^2 sv}{L} \left[3 + \frac{\tanh^{-1}\left(\frac{2\sqrt{2}}{3}\right)}{2\sqrt{2}} \right] \quad (28)$$

The total work for the translational motion of the tracer particle by a linear displacement s is finally given by

$$W_s = \frac{\pi a^2}{L} [Gs^2 + 2\eta sv] \left[3 + \frac{\tanh^{-1}\left(\frac{2\sqrt{2}}{3}\right)}{2\sqrt{2}} \right] \quad (29)$$

Thus, eq 29 has two stress contributions to the total work: the first one is due to the shear τ_{\parallel} , and the second one is due to the compression/extension of the matrix τ_{\perp} .

B.2. Rotational Displacement by an Angle σ . Now let us analyze the rotational displacement as shown in Figure 8. During this motion only shear strain is experienced by the medium. If the probe rotates by angle σ about the z -axis, an infinitesimal element of surface area dA experiences a tangential displacement of magnitude $\sigma a \sin \theta$ and, thus, shears the medium by $\sigma a \sin \theta/L$. Taking into account the same considerations as for the translational displacement, the

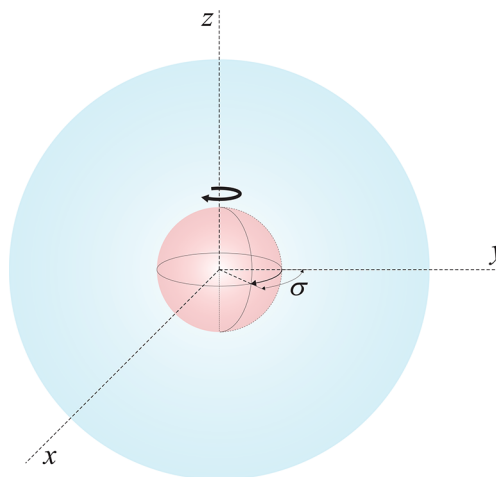


Figure 8. Probe has executed a rotation by an angle σ around the z -axis inside a medium with shear modulus G and shear viscosity η .

total force exerted on a surface element dA during the displacement by angle σ is given by

$$dF_{\sigma} = \tau_{\parallel} dA \quad (30)$$

The elastic and viscous contributions to the shear stress can be expressed as

$$\tau_{\parallel}^{(E)} = \gamma_{\parallel} G = G \frac{\sigma a \sin \theta}{L} \quad (31)$$

$$\tau_{\parallel}^{(V)} = \eta \dot{\gamma}_{\parallel} = \eta \frac{\omega a \sin \theta}{L} \quad (32)$$

where ω is the angular velocity of the tracer. Combining eqs 30 and 31, for the elastic contribution the force can be rewritten as

$$dF_{\sigma}^{(E)} = G \frac{\sigma a \sin \theta}{L} a^2 \sin \theta d\theta d\phi \quad (33)$$

Combining eqs 30 and 32, for the viscous contribution the force is

$$dF_{\sigma}^{(V)} = \eta \frac{\omega a \sin \theta}{L} a^2 \sin \theta d\theta d\phi \quad (34)$$

Integration of eqs 33 and 34 yields

$$F_{\sigma}^{(E)} = G \frac{\sigma a^3}{L} \int_{\theta=0}^{\theta=\pi} \int_{\phi=0}^{\phi=2\pi} \sin^2 \theta d\theta d\phi \quad (35)$$

$$F_{\sigma}^{(V)} = \eta \frac{\omega a^3}{L} \int_{\theta=0}^{\theta=\pi} \int_{\phi=0}^{\phi=2\pi} \sin^2 \theta d\theta d\phi \quad (36)$$

The work is obtained by integration of eqs 35 and 36. Thus, the work for the elastic contribution is

$$W_{\sigma}^{(E)} = G \frac{2\pi\sigma a^3}{L} \int_{\theta=0}^{\theta=\pi} \int_{s=0}^{s=\sigma a \sin \theta} \sin^2 \theta ds d\theta \quad (37)$$

$$= G \frac{8\pi\sigma^2 a^4}{3L} \quad (38)$$

and for the viscous contribution is

$$W_{\sigma}^{(V)} = \eta \frac{2\pi\omega a^3}{L} \int_{\theta=0}^{\theta=\pi} \int_{s=0}^{s=\sigma a \sin \theta} \sin^2 \theta ds d\theta \quad (39)$$

$$= \eta \omega \frac{8\pi\sigma a^4}{3L} \quad (40)$$

The total work due to the rotational motion of the tracer particle is finally given by

$$W_{\sigma} = \frac{8\pi a^4}{3L} [G\sigma^2 + \eta\sigma\omega] \quad (41)$$

Therefore, only shear stress τ_{\parallel} contributes to the total work.

B.3. Translational and Rotational Work Ratio. The work ratio is obtained by dividing eq 29 by eq 41. The translational work differs from the rotational work by a factor of

$$\frac{W_s}{W_{\sigma}} = \frac{3C}{8a^2} \left(\frac{G_T s^2 + 2\eta_T s v}{G_R \sigma^2 + \eta_R \sigma \omega} \right) \quad (42)$$

where subindices T and R mean “detected” by tracer translation and rotation, respectively. The coefficient C is

$$C = 3 + \frac{\tanh^{-1}\left(\frac{2\sqrt{2}}{3}\right)}{2\sqrt{2}} \approx 3.623 \quad (43)$$

According to this ratio, the difference between translation and rotation is due to the contribution of the normal stress (polymer gel compression/extension) to the total force acting on a particle. Compression, as well as partial slipping between a particle and the polymer chains, may result in an underestimation of the viscoelastic moduli probed by translational motion.^{25,54} In terms of our theoretical model, if the polymer matrix is highly compressible, then for translational motion Young's modulus must be substituted in terms of G using another suitable relationship, whereas W_{σ} does not involve Y and is unaffected by compression.

B.4. Storage and Loss Moduli for a Kelvin–Voigt Medium.

To calculate the work ratio for real experimental systems such as PAA networks or xanthan solutions, it is necessary to express eq 42 in terms of experimentally measurable quantities such as the frequency-dependent storage modulus $G'(\omega)$ and loss modulus $G''(\omega)$. We use the Kelvin–Voigt model for the viscoelastic medium. Gelatin hydrogels have been successfully modeled as Kelvin–Voigt fluids,⁵⁶ and other hydrogels such as gellan gum⁵⁷ and alginate and agarose constructs⁵⁸ have been successfully described using models based on the Kelvin–Voigt model. This model's main limitation is its inability to describe long-term relaxation, but since we examine intermediate times, this is not a fatal flaw for our purposes. Thus, we have

$$G'(\omega) = G \quad (44)$$

$$G''(\omega) = \omega \eta \quad (45)$$

Then eq 42 can be expressed as

$$\left[\frac{W_s}{W_{\sigma}} \right]_{\text{KV}} = \frac{3C}{8a^2\omega} \left[\frac{s^2\omega G'_T(\omega) + 2svG''_T(\omega)}{\sigma^2 G'_R(\omega) + \sigma G''_R(\omega)} \right] \quad (46)$$

Because work W is approximately proportional (eqs 29 and 41) while the complex moduli G^* are inversely proportional (eqs 4 and 5) to the square displacement, the work ratio is then related to the moduli ratio as follows:

$$\frac{W_s}{W_{\sigma}} \sim \frac{G_R^*}{G_T^*} \quad (47)$$

Figure 9 shows the work ratios for both PAA networks and xanthan solutions as a function of f_{bis} or the polysaccharide concentration. As shown in Figure 9, the work ratios for both systems are larger than 1000 (value of the work ratio when $G'_R = G'_T$ and $G''_R = G''_T$) for the majority of samples, and they increase with increasing f_{bis} or xanthan concentration. Taking eq 47 into account, Figure 9 qualitatively reproduces Figure 5. Therefore, the theory reproduces the experimental behavior quite well. The variation of W_s/W_{σ} on increase of viscoelasticity of the system represents the degree of diffusion decoupling. At the three largest f_{bis} the degree of decoupling stays constant indicating similarity in the hindering of the tracer dynamics. This is not the case for xanthan, since the work ratio increases up to the largest polymer concentration studied. All four data sets have correlations with p -values (the probability that random variations would produce a correlation no smaller than the value obtained) such that the correlations are very statistically significant by conventional criteria, which is inconsistent with the variation in the work ratios being the

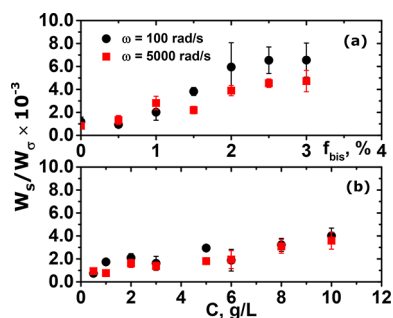


Figure 9. Work ratios due to translational (W_s) and rotational (W_r) motion of the tracers: (a) on variation of the cross-linker mass fraction f_{bis} in PAA networks and (b) on variation of xanthan concentration in solutions. The values are calculated at frequencies of 100 (circles) and 5000 rad/s (squares). Error bars correspond to approximate uncertainties. All four data sets have correlation coefficients >0.8 and p -values <0.01 .

result of random experimental error but is consistent with this variation having a physical origin.

Because work is an increasing function of the displacement, larger work implies larger tracer displacement; namely, the tracer can translate more easily than it can rotate. The fit parameters of a certain mathematical function to the increasing work ratios might potentially represent the rate of diffusion decoupling for each system. Decoupling appears to increase more rapidly for PAA systems.

For the most cross-linked or concentrated systems, their behavior should be governed overwhelmingly by the elastic contribution—even treating these systems as elastic solids would be expected to be a reasonable approximation, so even if the Kelvin–Voigt model imperfectly captures the viscosity’s contribution to the overall behavior, this cannot on its own account for the large discrepancies in the apparent moduli nor for the large work ratios. The discrepancy is clearly both large and depends on cross-linker mass fraction or xanthan concentration, as does the work ratio (see Figures 5 and 9). The weakest assumption in the foregoing equations is that each individual particle is assumed to probe a stable, homogeneous region. However, Stillinger and Hodgdon⁵⁹ developed a model for supercooled liquids, assuming them to have time-dependent fluidlike and solidlike domains, which predicts translational (but not rotational) microrheology yields of viscosity to deviate from the bulk viscosity by 2 orders of magnitude for the fluids examined. It is plausible that our systems exhibit qualitatively similar behavior, i.e., also exhibit time-dependent fluidlike and solidlike domains, the model’s key assumptions.⁵⁹ Polyacrylamide gels are known to exhibit large dynamic heterogeneities,¹⁸ and xanthan’s tendency to form aggregates makes dynamic heterogeneities highly probable. Extending this argument to complex viscosity could account for the discrepancy between the rotational and the translational results.

In addition, the polymer networks might not be approximately weakly compressible. If the assumption of weak compressibility does not hold, since translational displacement involves both Young’s modulus and the shear modulus, as it inherently involves both extensional and shear deformation of the medium, then W_s is not as described by eqs 23–29, whereas W_r is unaffected. Because both compressibility (and therefore the relationship between Young’s modulus and the shear modulus) and the nature of dynamic heterogeneities

(including time dependence) likely depend on the degree of cross-linking or on xanthan concentration, these effects can account for these parameters and the work ratios being correlated.

IV. CONCLUSIONS

We present an experimental and theoretical study of the discrepancies of microscopic viscoelastic properties observed by translational and rotational microrheology. These discrepancies stem from the decoupling of translational and rotational diffusion of spherical probe particles inside an entangled matrix independently of the matrix nature. The tracer diffusion decoupling is enhanced by growing matrix rigidity and slowdown of its dynamics. The theory predicts that the tracer rotation within the matrix slows down faster than its translation when its motion in the viscoelastic medium is treated using the no-slip condition. The theoretical description is in a good qualitative agreement with the experimental results. The theory developed explains the moduli discrepancies in terms of the different stress contributions of tracer translation and rotation, as the former involves normal stresses. Thus, if the polymer matrix’s compressibility is unknown, its microrheology is best determined by tracer rotational motion; on the other hand, translational microrheology may yield valuable insights into the polymer matrix’s compressibility.

■ ASSOCIATED CONTENT

Supporting Information

The Supporting Information is available free of charge on the ACS Publications website at DOI: 10.1021/acs.macromol.8b01005.

Figures S1–S7 (PDF)

■ AUTHOR INFORMATION

Corresponding Author

*E-mail: akozina@unam.mx (A.K.).

ORCID

Anna Kozina: 0000-0002-4287-2953

Notes

The authors declare no competing financial interest.

■ ACKNOWLEDGMENTS

Financial support from CONACyT (grants INFR 163241, CB 238618, CB 256599 and FC 1450) and DGAPA-UNAM (IA 100217) is gratefully acknowledged.

■ REFERENCES

- (1) Mason, T. G.; Weitz, D. A. Optical Measurements of Frequency-Dependent Linear Viscoelastic Moduli of Complex Fluids. *Phys. Rev. Lett.* **1995**, *74*, 1250.
- (2) Mason, T. G. Estimating the Viscoelastic Moduli of Complex Fluids Using the Generalized Stokes-Einstein equation. *Rheol. Acta* **2000**, *39*, 371.
- (3) Dasgupta, B. R.; Tee, S.-Y.; Crocker, J. C.; Frisken, B. J.; Weitz, D. A. Microrheology of Polyethylene Oxide using Diffusing Wave Spectroscopy and Single Scattering. *Phys. Rev. E: Stat. Phys., Plasmas, Fluids, Relat. Interdiscip. Top.* **2002**, *65*, 051505.
- (4) Harden, J. L.; Viasnoff, V. Recent Advances in DWS-based Micro-rheology. *Curr. Opin. Colloid Interface Sci.* **2001**, *6*, 438.
- (5) Moschakis, T.; Murray, B. S.; Dickinson, E. Particle Tracking Using Confocal Microscopy to Probe the Microrheology in a Phase-separating Emulsion Containing Nonadsorbing Polysaccharide. *Langmuir* **2006**, *22*, 4710.

- (6) Cardinaux, F.; Cipelletti, L.; Scheffold, F.; Schurtenberger, P. Microrheology of Giant-micelle Solutions. *Europhys. Lett.* **2002**, *57*, 738.
- (7) Appar, J.; Tseng, Y.; Fedorov, E.; Herwig, M. B.; Almo, S. C.; Wirtz, D. Multiple-Particle Tracking Measurements of Heterogeneities in Solutions of Actin Filaments and Actin Bundles. *Biophys. J.* **2000**, *79*, 1095.
- (8) Cheng, Z.; Mason, T. G. Rotational Diffusion Microrheology. *Phys. Rev. Lett.* **2003**, *90*, 018304.
- (9) Díaz-Leyva, P.; Pérez, E.; Arauz-Lara, J. L. Dynamic Light Scattering by Optically Anisotropic Colloidal Particles in Polyacrylamide Gels. *J. Chem. Phys.* **2004**, *121*, 9103.
- (10) Andablo-Reyes, E.; Díaz-Leyva, P.; Arauz-Lara, J. L. Microrheology from Rotational Diffusion of Colloidal Particles. *Phys. Rev. Lett.* **2005**, *94*, 106001.
- (11) Haro-Pérez, C.; Andablo-Reyes, E.; Díaz-Leyva, P.; Arauz-Lara, J. L. Microrheology of Viscoelastic Fluids Containing Light-scattering Inclusions. *Phys. Rev. E* **2007**, *75*, 041505.
- (12) Waigh, T. A. Microrheology of Complex Fluids. *Rep. Prog. Phys.* **2005**, *68*, 685.
- (13) Mason, T. G.; Gang, H.; Weitz, D. A. Rheology of Complex Fluids Measured by Dynamic Light Scattering. *J. Mol. Struct.* **1996**, *383*, 81–90.
- (14) Schnurr, B.; Gittes, F.; MacKintosh, F. C.; Schmidt, C. F. Determining Microscopic Viscoelasticity in Flexible and Semiflexible Polymer Networks from Thermal Fluctuations. *Macromolecules* **1997**, *30*, 7781–7792.
- (15) Gardel, M. L.; Valentine, M. T.; Crocker, J. C.; Bausch, A. R.; Weitz, D. A. Microrheology of Entangled F-Actin Solutions. *Phys. Rev. Lett.* **2003**, *91*, 158302.
- (16) Sarmiento-Gomez, E.; Montalvan-Sorrosa, D.; Garza, C.; Mas-Oliva, J.; Castillo, R. Rheology and DWS Microrheology of Concentrated Suspensions of the Semiflexible Filamentous fd Virus. *Eur. Phys. J. E: Soft Matter Biol. Phys.* **2012**, *35*, 35.
- (17) Kozina, A.; Díaz-Leyva, P.; Friedrich, C.; Bartsch, E. Structural and Dynamical Evolution of Colloid-polymer Mixtures on Crossing Glass and Gel Transition as seen by Optical Microrheology and Mechanical Bulk Rheology. *Soft Matter* **2012**, *8*, 1033.
- (18) Dasgupta, B. R.; Weitz, D. A. Microrheology of Cross-linked Polyacrylamide Networks. *Phys. Rev. E* **2005**, *71*, 021504.
- (19) Lu, Q.; Solomon, M. J. Probe Size Effects on the Microrheology of Associating Polymer Solutions. *Phys. Rev. E: Stat. Phys., Plasmas, Fluids, Relat. Interdiscip. Top.* **2002**, *66*, 061504.
- (20) Mizuno, D.; Head, D. A.; MacKintosh, F. C.; Schmidt, C. F. Active and Passive Microrheology in Equilibrium and Nonequilibrium Systems. *Macromolecules* **2008**, *41*, 7194.
- (21) Pashkovski, E. E.; Masters, J. G.; Mehreteab, A. Viscoelastic Scaling of Colloidal Gels in Polymer Solutions. *Langmuir* **2003**, *19*, 3589.
- (22) Amin, S.; Rega, C. A.; Jankevics, H. Detection of Viscoelasticity in Aggregating Dilute Protein Solutions through Dynamic Light Scattering-based Optical Microrheology. *Rheol. Acta* **2012**, *51*, 329.
- (23) Grabowski, C. A.; Mukhopadhyay, A. Size Effect of Nanoparticle Diffusion in a Polymer Melt. *Macromolecules* **2014**, *47*, 7238.
- (24) Chen, D. T.; Weeks, E. R.; Crocker, J. C.; Islam, M. F.; Verma, R.; Gruber, J.; Levine, A. J.; Lubensky, T. C.; Yodh, A. G. Rheological Microscopy: Local Mechanical Properties from Microrheology. *Phys. Rev. Lett.* **2003**, *90*, 108301.
- (25) Fu, H. C.; Shenoy, V. B.; Powers, T. R. Role of Slip between a Probe Particle and a Gel in Microrheology. *Phys. Rev. E* **2008**, *78*, 061503.
- (26) Chae, B. S.; Furst, E. M. Probe Surface Chemistry Dependence and Local Polymer Network Structure in F-Actin Microrheology. *Langmuir* **2005**, *21*, 3084.
- (27) Fujara, F.; Geil, B.; Sillescu, H.; Fleischer, G. Translational and Rotational Diffusion in Supercooled Orthoterphenyl close to the Glass Transition. *Z. Phys. B: Condens. Matter* **1992**, *88*, 195.
- (28) Chong, S.-H.; Kob, W. Coupling and Decoupling between Translational and Rotational Dynamics in a Supercooled Molecular Liquid. *Phys. Rev. Lett.* **2009**, *102*, 025702.
- (29) Edmond, K. V.; Elsesser, M. T.; Hunter, G. L.; Pine, D. J.; Weeks, E. R. Decoupling of Rotational and Translational Diffusion in Supercooled Colloidal Fluids. *Proc. Natl. Acad. Sci. U. S. A.* **2012**, *109*, 17891.
- (30) Vivek, S.; Weeks, E. R. Decoupling of Translational and Rotational Diffusion in Quasi-2D Colloidal Fluids. *J. Chem. Phys.* **2017**, *147*, 134502.
- (31) Kim, M.; Anthony, S. M.; Bae, S. C.; Granick, S. Colloidal Rotation near the Colloidal Glass Transition. *J. Chem. Phys.* **2011**, *135*, 054905.
- (32) Park, Y.; Kim, J.; Sung, B. J. Translation-Rotation Decoupling of Tracers of Locally Favorable Structures in Glass-Forming Liquids. *J. Chem. Phys.* **2017**, *147*, 124503.
- (33) Liang, M.; Harder, R.; Robinson, I. K. Brownian Motion Studies of Viscoelastic Colloidal Gels by Rotational Single Particle Tracking. *IUCrJ.* **2014**, *1*, 172.
- (34) Koenderink, G. H.; Sacanna, S.; Aarts, D. G. A. L.; Philipse, A. P. Rotational and Translational Diffusion of Fluorocarbon Tracer Spheres in Semidilute Xanthan Solutions. *Phys. Rev. E* **2004**, *69*, 021804.
- (35) Viebke, C. OrderDisorder Conformational Transition of Xanthan Gum. In *Polysaccharides: Structural Diversity and Functional Versatility*; Dumitriu, S., Ed.; Marcel Dekker: 2005.
- (36) Merino-González, A.; Kozina, A. Influence of Aggregation on Characterization of Dilute Xanthan Solutions. *Int. J. Biol. Macromol.* **2017**, *105*, 834.
- (37) Hsu, M. F.; Dufresne, E. R.; Weitz, D. A. Charge Stabilization in Nonpolar Solvents. *Langmuir* **2005**, *21*, 4881.
- (38) Roberts, G. S.; Sanchez, R.; Kemp, R.; Wood, T.; Bartlett, P. Electrostatic Charging of Nonpolar Colloids by Reverse Micelles. *Langmuir* **2008**, *24*, 6530.
- (39) Mertelj, A.; Arauz-Lara, J. L.; Maret, G.; Gisler, T.; Stark, H. Rotational Diffusion in a Bistable Potential. *Europhys. Lett.* **2002**, *59*, 337.
- (40) Maurer, H. R. *Disk Gel Electrophoresis*; de Gruyter: Berlin, 1971.
- (41) Nishio, I.; Reina, J. C.; Bansil, R. Quasielastic Light-Scattering Study of the Movement of Particles in Gels. *Phys. Rev. Lett.* **1987**, *59*, 684.
- (42) Berne, B. J.; Pecora, R. *Dynamic Light Scattering: With Applications to Chemistry, Biology and Physics*; John Wiley & Sons: New York, 1976.
- (43) Pusey, P. N.; van Megen, W. Dynamic Light Scattering by Non-ergodic Media. *Phys. A* **1989**, *157*, 705.
- (44) Zero, K.; Pecora, R. In *Dynamic Depolarized Light Scattering in Dynamic Light Scattering*; Pecora, R., Ed.; Plenum Press: New York, 1985.
- (45) Milas, M.; Rinaudo, M.; Knipper, M.; Schuppiser, J. L. Flow and Viscoelastic Properties of Xanthan Gum Solutions. *Macromolecules* **1990**, *23*, 2506.
- (46) Song, K.-W.; Kuk, H.-Y.; Chang, G.-S. Rheology of Concentrated Xanthan Gum Solutions: Oscillatory Shear Flow Behavior. *Korea-Austr. Rheol. J.* **2006**, *18*, 67.
- (47) Choppe, E.; Puaud, F.; Nicolai, T.; Benyahia, L. Rheology of Xanthan Solutions as a Function of Temperature, Concentration and Ionic Strength. *Carbohydr. Polym.* **2010**, *82*, 1228.
- (48) Wyatt, N. B.; Gunther, C. M.; Liberatore, M. W. Increasing Viscosity in Entangled Polyelectrolyte Solutions by the Addition of Salt. *Polymer* **2011**, *52*, 2437.
- (49) Otsubo, Y.; Umeya, K. Adsorption of Polyacrylamide on Silica Particles and Its Effect on the Rheological Properties of Suspensions. *J. Colloid Interface Sci.* **1983**, *95*, 279.
- (50) Furusawa, K.; Shou, Z.; Nagahashi, N. Polymer Adsorption on Fine Particles; the Effects of Particle Size and its Stability. *Colloid Polym. Sci.* **1992**, *270*, 212.
- (51) McGuire, M. J.; Addai-Mensah, J.; Bremmell, K. E. Spectroscopic Investigation of the Adsorption Mechanisms of

Polyacrylamide Polymers onto Iron Oxide Particles. *J. Colloid Interface Sci.* **2006**, *299*, 547.

(52) Sato, N.; Aoyama, Y.; Yamanaka, J.; Toyotama, A.; Okuzono, T. Particle Adsorption on Hydrogel Surfaces in Aqueous Media due to van der Waals Attraction. *Sci. Rep.* **2017**, *7*, 6099.

(53) Cooper, E. C.; Johnson, P.; Donald, A. M. Probe Diffusion in Polymer Solutions in the Dilute/Semi-dilute Crossover Regime: 1. Poly(ethylene oxide). *Polymer* **1991**, *32*, 2815.

(54) Diamant, H. Response of a Polymer Network to the Motion of a Rigid Sphere. *Eur. Phys. J. E: Soft Matter Biol. Phys.* **2015**, *38*, 32.

(55) Mott, P. H.; Roland, C. M. Limits to Poissons Ratio in Isotropic Materials. *Phys. Rev. B: Condens. Matter Mater. Phys.* **2009**, *80*, 132104.

(56) Shabaniverki, S.; Juárez, J. J. Characterizing Gelatin Hydrogel Viscoelasticity with Diffusing Colloidal Probe Microscopy. *J. Colloid Interface Sci.* **2017**, *497*, 73.

(57) Kocen, R.; Gasik, M.; Gantar, A.; Novak, S. Viscoelastic Behaviour of Hydrogel-Based Composites for Tissue Engineering under Mechanical Load. *Biomed. Mater.* **2017**, *12*, 025004.

(58) Ahearne, M.; Yang, Y.; el Haj, A. J.; Then, K. Y.; Liu, K.-K. Characterizing the Viscoelastic Properties of Thin Hydrogel-Based Constructs for Tissue Engineering Applications. *J. R. Soc., Interface* **2005**, *2*, 455.

(59) Stillinger, F. H.; Hodgdon, J. A. Translation-Rotation Paradox for Diffusion in Fragile Glass-Forming Liquids. *Phys. Rev. E: Stat. Phys., Plasmas, Fluids, Relat. Interdiscip. Top.* **1994**, *50*, 2064.